IEEE Access
Multidisciplinary | Rapid Review | Open Access Journal

Received September 15, 2020, accepted September 28, 2020, date of publication October 14, 2020,
date of current version November 4, 2020.

Digital Object Identifier 10.1109/ACCESS.2020.3030848

Normal-Based Flower Pollination Algorithm (FPA) for Solving 3D Point Set Registration via Rotation Optimization

DING SHEN[1,2], YOUXI LIN[1], ZHIYING REN[1,3], AND WEIPING CHEN[1]
[1]School of Mechanical Engineering and Automation, Fuzhou University, Fuzhou 350106, China
[2]Fujian Metrology Institute, Fuzhou 350003, China
[3]Military Engineering Innovation Center for Knitted Wire Mesh of Fujian Province, Fuzhou University, Fuzhou 350106, China

Corresponding authors: Youxi Lin (youthlin@fzu.edu.cn) and Zhiying Ren (renzyrose@126.com)

This work was supported in part by the National Natural Science Foundation of China under Grant 51805086 and Grant 51975123, in part by the Fujian Provincial Natural Science Foundation under Grant 2019J01210, in part by the Fujian Province Health Education Joint Project under Grant 2019-WJ-01; and in part by the Fuzhou Science and Technology Plan Project under Grant 2019-G-42.

ABSTRACT Compared with the registration methods based on local optimizations, the heuristic registration methods are less sensitive to the initial position, and a reasonable bound range is essential to ensure the registration validity. In practice, compared with a rotation bound range, which is periodic, the setting of the translation range is more difficult and manual interventions required, especially when the initial position is complex. Moreover, it has yet to be discussed in past research. Therefore, a normal-based registration method based on the flower pollination algorithm is proposed in this paper, in which only rotation parameters (r_x, r_y, r_z) are considered. In our method, the point correspondences are guided by their normal due to their invariance to position translation. Considering the normal degeneration caused by noise, outliers, and partial overlapping, the Pauta criterion is employed to remove distorted correspondences and acquire reliable translation. Moreover, the population of optimal pollens is guaranteed by the use of the searching radius adjustment and periodic boundary. A number of experiments demonstrate that the proposed method exhibits competitive or better performance in terms of initial position, noise, outliers and partial overlapping. Furthermore, a real quality inspection is also implemented to confirm the availability and superiority of the proposed method in the manufacturing process.

INDEX TERMS Iterative closest points (ICP), heuristic registration method, flower pollination algorithm, Pauta criterion, quality inspection.

I. INTRODUCTION

As a critical process in computer vision, biomedical imaging, and quality inspection, the goal of registration is to align the point sets in different coordinates [1]–[3]. In rigid point registration, the optimal Euclidean motion is required to match different models as closely as possible. Compared with manual intervention, automatic matching is a hot topic in the last decades. Considering efficiency and registration accuracy, the whole process can be divided into coarse registration and fine registration [4]. Generally, the geometrical characteristics of the model are used to realize rough alignment, and a more precise Euclidean motion is obtained to minimize the distance between the models in fine registration.

The associate editor coordinating the review of this manuscript and approving it for publication was Joewono Widjaja.

According to the optimization strategy involved in registration, the registration method can be divided into local optimal algorithm and heuristic method. Due to stochastic searching ability, when the initial position is complex, the heuristic method has a higher potential than convex optimization method in finding the global optimum. Generally, in 3D rigid registration, the heuristic method needs to find the optimal transformation parameters $[r_x, r_y, r_z, t_x, t_y, t_z]$ to achieve perfect match in the search range, where $r.$ and $t.$ denote the rotation and translation along the $\cdot$ axis. The pre-setting of the search range is still an experimental work, and human intervention is required. To ensure perfect alignment, the search range of the heuristic registration method is different in related researches due to the differences in model dimensions and applications, especially for the search range of the translation parameters $[t_x, t_y, t_z]$.

For example, in prior studies [5]–[7], the search range of t. was [−(0.001∼0.01)L, (0.001∼0.01)L] to achieve full-overlapping registration, where L denotes the max dimension of model in their studies. In other studies [8], [9], the translation range was artificially limited to [−40mm, 40mm] for partial-overlapping registration. In Fig. 1, to illustrate the influence of translation range and initial position to the convergence results, the heuristic registration of bunny model is taken for an example, which is also used in the later experiment. When the initial position is more complex, the translation space should be broader to ensure the global optimal parameters in the default space. However, it is difficult for heuristic methods to find the global optimal solution in an extensive range.

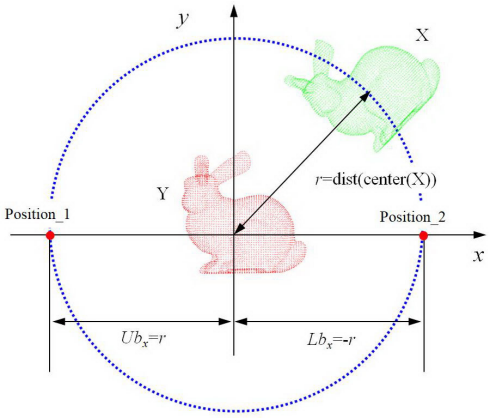

(a) Analysis of translation search space

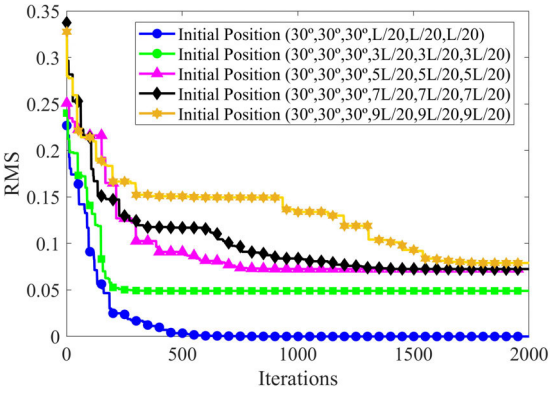

(b) Convergence result of Flower pollination algorithm

FIGURE 1. The analysis of heuristic convergence. Here, we use FPA to align the point set X (green) to Y (red) in Fig 1a. The rotation range is [−180°, 180°], and the translation space should be [-dist(center(X)), dist(center(X))] for full-overlapping registration. Considering the disturbance of noise, outliers, occlusion, and clutter in partial overlapping, the translation search space should be enlarged as t. ∈[-dist(center(X))−0.5L, dist(center(X))+0.5L], where center (·) and dist (·) denote the geometric center and the distance-to-origin operator, respectively.

To reduce the optimization dimensions in the 3D registration problem, the point set normal is adopted to acquire point correspondences in different models. Considering the normal deterioration caused by noise, outliers, occlusion and clutter in partial overlapping, the point normal comes from the eigenvector of the neighbors' covariance matrix, and the Pauta criterion in vectorization is adopted to acquire reliable correspondences as well as the translation between the models. In addition, the adjustment of searching radius and periodic boundary are introduced into FPA to increase the populations of optimal pollen. Finally, the modified FPA is used to find optimal parameters $(r_x, r_y, r_z)_{\text{optimal}}$ in the rotation range to solve 3D registration problems.

II. PREVIOUS WORK

Recently, the iterative closest points (ICP) algorithm, optimizations based on a probability density function (PDF), and heuristic algorithms have often been employed in registration [10]–[12]. In general, the ICP algorithm is more efficient than other methods. However, its sensitivity to noise, outliers, and initial position still bother users. Consequently, several variants have been proposed by scholars [13], [14]. To weaken the dependency on the initial position, a branch and bound (BnB) strategy was introduced to explore optimal Euclidean transformation [15]. Recently, a semi-definite and relaxation method was used in the stochastic sampling objective function to fulfill model alignment when initial position is complex [16]. A mutual matching based on dynamical adaptation between the color and the spatial information was used to estimate transformation parameters [17]. Compared with ICP, registration based on a probability density function (PDF) is more robust to noise and outliers. Besides the application in rigid registration, the PDF-based methods, such as coherent point drift (CPD) and Gaussian mixture model registration (GMM-REG), can also fulfill non-rigid alignments [11], [19]. The dynamic programming algorithm was introduced into the method to find optimal feature candidates and fulfill non-rigid registration [18]. Although the PDF-based methods are less sensitive to the initial position, it is also difficult for them to calculate the global optimal solution when the registration parts are far away. In recent years, heuristic optimization has been widely used in model registration, and the related works have been substantially increased [8]. In heuristic methods, a bio-inspired or population-based strategy is used to search for the global optimal solution in the default range. To solve registration problems appropriately, modified versions have been proposed. Jacq and Roux applied genetic algorithm (GA) to realize non-rigid transformation between the volumetric maps of 3D medical images [20]. Brunnstrom. *et al.* used GA to find an initial guess for further refinement [21]. Considering the great computation involved in the optimizing process, a parallel implementation of GA was proposed in prior work, but at the cost of registration accuracy [22]. Dally and Flynn suggested that good registration should present the maximum interpenetration between aligned surfaces [23]. Given this, Silva *et al.* proposed a hybrid genetic method combined with a hill-climbing algorithm to maximize the surface interpenetration measure (SIM) [24]. Using the median square error as an objective function, Cordon *et al.* conducted in-depth

studies in range image registration based on heuristic optimizations, such as self-evolutionary algorithm (SaEVO), artificial bee colony (ABC), harmony search (HS), and scatter search (SS) [9]. Combined with restart and dynamic boundary mechanisms with a multi-resolution strategy, an improved scatter search algorithm was proposed to fulfill intensity-based medical image registration [25]. Based on a cost function of mutual information, the differential evolution (DE) was used to realize the affine transformation between the 2D satellite images [26]. In quality inspection of free-form surface, He *et al.* proposed a DE hybrid approach to address profile error evaluation [27]. Recently, Li *et al.* did many researches in quality inspection based on heuristic optimizations, such as DE and fruit fly optimization (FFO) and its variants [5]–[7]. Incorporated with an ICP-based initialization strategy, an ensemble FFO was put forward to realize alignment between the scanned model and its computer-aided design (CAD) model [5]. A DE-based registration method was introduced to achieve the registration of point sets, which was simplified by the directed hausdorff distance (DHD) [6]. To strengthen the global searching ability of the heuristic algorithm, the FFO was combined with the saccade factor to evaluate profile errors [7].

Many registration methods based on heuristic optimization are aimed at finding optimal transformation parameters, even when the initial position is complex. However, the registration result is easy to degenerate when the translation between models is taken into consideration. And compared with rotation space, the setting of the translation solution space is difficult and intervention-required. In our method, the translation vector can be deduced by the point correspondences. There is no need for users to find a reasonable translation space before registration.

III. PROPOSED METHOD

Firstly, the traditional heuristic registration method (six-dimensional optimization) is reviewed to provide a distinction between it and the proposed method.

A. TRADITIONAL REGISTRATION METHOD

In the traditional registration method, the appropriate rotation matrix $R \in SO(3)$ and translation vector $T \in R^3$ are required to align the source point set X ($X=\{x_i | x_i \in R^3, i=1, \cdots, N_x\}$) to target point set Y=$\{y_j | y_j \in R^3, j = 1, \cdots, N_y\}$. The N_x and N_y are the number of points in point sets X and Y respectively. The process of registration can be expressed as follows:

$$f\left(y_{closet}(i, R, T), x_i(R, T)\right) \rightarrow \min \quad i = 1 \cdots N_x \tag{1}$$

$$y_{closet}(i, R, T) = \arg\min_{y \in Y} \|y - x_i(R, T)\| \tag{2}$$

where, $||\cdot||$ stands for the Euclidean norm. In most cases, the root mean square error (RMSE) can be used as an objective function f. To solve the objective function, singular value decomposition (SVD), Gauss-Newton method, and the Levenberg-Marquardt (LM) method can be applied in local optimization [10], [28]–[30]. For global optimization methods, the optimal parameters $(r_x, r_y, r_z, t_x, t_y, t_z)_{\text{optimal}}$ can be found in the searching range with the help of a bio-inspired and population-based strategy. The relation between Euclidean transformation and $(r_x, r_y, r_z, t_x, t_y, t_z)$ can be written as follows:

$$\begin{aligned} R = & \begin{bmatrix} 1 & 0 & 0 \\ 0 & \cos(r_x) & \sin(r_x) \\ 0 & -\sin(r_x) & \cos(r_x) \end{bmatrix} \\ & \times \begin{bmatrix} \cos(r_y) & 0 & -\sin(r_y) \\ 0 & 1 & 0 \\ \sin(r_y) & 0 & \cos(r_y) \end{bmatrix} \\ & \times \begin{bmatrix} \cos(r_z) & \sin(r_z) & 0 \\ -\sin(r_z) & \cos(r_z) & 0 \\ 0 & 0 & 1 \end{bmatrix} \end{aligned} \tag{3}$$

$$T = [\, t_x \quad t_y \quad t_z \,]' \tag{4}$$

where, $\cdot'$ is the transpose operator, and $r.$ and $t.$ denote the rotation and translation along the $\cdot$ axis. Furthermore, kd-tree technology can be used as fast implementation for Eq. 2.

B. PROPOSED REGISTRATION METHOD

Traditionally, heuristic methods need to find optimal values in six-dimensional space. Moreover, it is necessary to predict the search space in advance. Compared with the rotation space, it is more difficult to preset the translation space, especially for partial-overlapping registration. In the proposed method, the optimal rotation parameters are only required to fulfill registration, and the whole process can be represented as follows:

$$\begin{aligned} & f\left(y_{closet}(i, R), x_i(R)\right) \\ & \quad = RMSE\left(x_i(R) + T, y_{closet\_D}(i, R)\right) \rightarrow \min \end{aligned} \tag{5}$$

$$T = mean\left[Pauta\left(y_{closet\_N}(i, R) - x_i(R)\right)\right] \tag{6}$$

$$y_{closet\_N}(i, R) = \arg\min_{y \in Y} \|normal(y) - normal\left(x_i(R)\right)\| \tag{7}$$

$$y_{closet\_D}(i, R) = \arg\min_{y \in Y} \|y - x_i(R) - T\| \tag{8}$$

where, $normal(\cdot)$ means the point-normal operator, and $Pauta(\cdot)$ stands for the Pauta operator, and its process is described in the following section, and $y_{closet\_N}(\cdot, R)$ and $y_{closet\_D}(\cdot, R)$ represent the closet point in point set Y with respect to normal distribution and distance respectively, when rotation matrix is R. The point normal would not be changed unless its direction is transformed by a rotation matrix. Therefore, they can be used to find the corresponding point in the target model. As described in Eq. 7, the Euclidean norm is employed to estimate the closeness of the point normal. It is feasible to use kd-tree to speed up the computation. To eliminate the influence from noise and outliers, the normal direction comes from the eigenvector of weighted covariance matrix M_{cor} [31], and the corresponding eigen-value is used as the norm of its normal to improve

discrimination

$$M_{cor}(x_i) = \frac{\left(\sum_{j}^{\|x_j - x_i\| \le radius} \left(radius - \|x_j - x_i\|\right)(x_j - x_i)(x_j - x_i)'\right)}{\sum_{j}^{\|x_j - x_i\| \le radius} \left(radius - \|x_j - x_i\|\right)} \tag{9}$$

$$normal(x_i) = \lambda_{\min} \overrightarrow{e_{\lambda \min}} \tag{10}$$

where $\lambda_{\min}$ and $\overrightarrow{e_{\lambda min}}$ are the minimum eigen-value and its eigenvector of matrix M_{cor}. Considering the computation burden and robustness to abnormalities, the support radius of M_{cor} is five times point resolution ($radius$=5mr). As mentioned in prior work [32], the signs of the eigenvectors are not repeatable even at the same mesh. To enhance the sign robustness, the eigenvector can be rewritten as the following function. (11), as shown at the bottom of the next page.

In Fig. 2, the points' location and their normal distribution are depicted.

FIGURE 2. The bun000 (red) and bun045 (green), and their point-normal distribution

C. CORRESPONDENCES REFINEMENT WITH THE PAUTA CRITERION

As illustrated in Eq. 6, the initial correspondences can be acquired from the normal closeness. However, the initial correspondences are unreliable, due to the normal degradation caused by noise, outliers, occlusion and clutter in scenes, as depicted in Fig.3*a*. As a classical method in statistics and metrology, the Pauta criterion is always used to pick out the outliers in the measuring data, subjected to normal distribution. According to the Pauta criterion, the measuring data, whose deviation to mean value μ exceeds k times of the standard deviation σ, can be regarded as the gross error and should be removed from original data, as shown in Fig. 4. Traditionally, the recommended value of coefficient k is 3, where the method is famous as the 3σ rule. The confidence probability of the truth value in confidence interval $[\mu - 3\sigma, \mu + 3\sigma]$ is 99.73%, and the gross error mainly located in intervals $[-\infty, \mu - 3\sigma]$ and $[\mu + 3\sigma, +\infty]$.

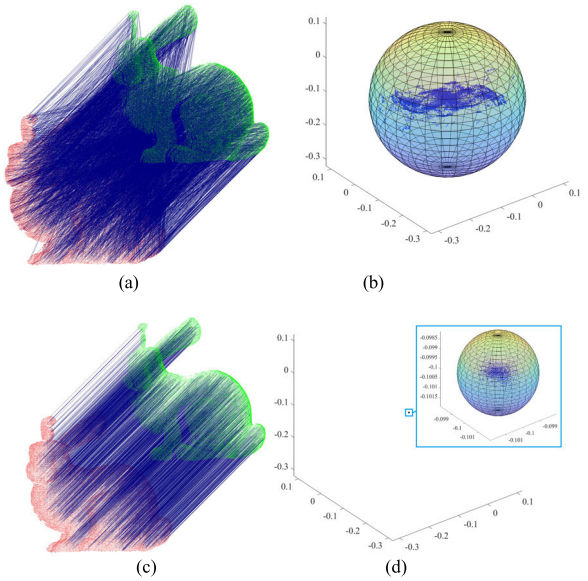

FIGURE 3. Analysis of heuristic convergence. (a) the point correspondence before filtering, (b) the endpoints of corresponding vectors before filtering, (c) the point correspondence after filtering, and (d) the endpoints of corresponding vectors after filtering.

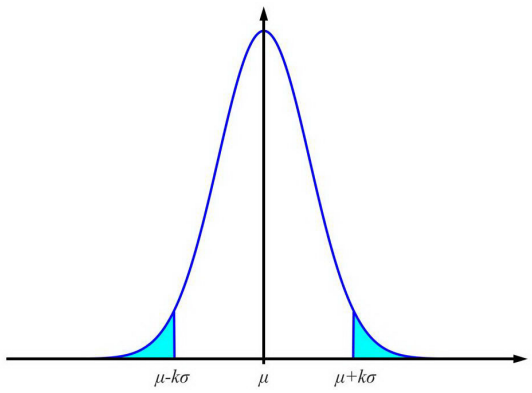

FIGURE 4. Probability density function of the normal distribution.

In rigid registration, when the rotation matrix $R(r_x, r_y, r_z)$ is appropriate, the corresponding vectors should be parallel and equal in norm. And it can be defined as

$$T = \overrightarrow{x_1 y_{x_{1_R}}} = \overrightarrow{x_2 y_{x_{2_R}}} = \cdots = \overrightarrow{x_i y_{x_{i_R}}} = \cdots = \overrightarrow{x_N y_{x_{N_R}}}, \tag{12}$$

where $\overrightarrow{x_i y_{xiR}} = y(x_i, R) - x_i(R)$, and T stands for the translation vector. We suppose that $\overrightarrow{x_i y_{xiR}}$ obeys to normal distribution, and the false correspondences are regarded as the gross error. Thus, the computation of translation vector T based on the Pauta criterion can be calculated as follows: where $\overrightarrow{xy}_{R,iter}$ and $\delta(\overrightarrow{xy}_{R,iter})$ are the set of corresponding vectors and corresponding standard deviation, and T_{iter} and N_{iter} are the translation vector and the number of valuable matches in $iter$-th iteration. As depicted in Fig. 3*a*, the initial correspondences are represented in a blue line, where $R(r_x, r_y, r_z) = R_{bench}$. Their corresponding vectors are demonstrated in Fig. 3b. And for the sake of observation, only

the endpoints of the vector are drawn in figure. To derive the efficient value of k for registration, the bunny scenes (Fig. 15a), whose overlapping ratio is larger than 40%, are recruited here. As shown in Fig. 5, when the confidence probability $P([\mu-k\sigma, \mu + k\sigma])$ is larger than 0.9, the registration precision dropped significantly. It means that the false matches involved in correspondences are grow, and the translation error ΔT becomes larger. As shown in Fig. 6b, the translation error ΔT is the largest, when confidence probability $P([\mu-k\sigma, \mu + k\sigma])$ is 0.9973 ($k = 3$). And the smaller the confidence probability is, the higher the corresponding precision (Figure 5). However it may give rise to a slight increase in the translation errors ΔT, due to the fewer participants involved in registration (Fig. 6a). As shown in Fig. 6b, when confidence probability is less than 0.85, the translation error ΔT between convergence translation and benchmark becomes larger. Thus, the confidence probability selected in this paper is 0.9 ($P([\mu-k\sigma, \mu + k\sigma]) = 0.9$), whose corresponding coefficient k is 1.645. For example, the correspondences and their vectors (bun_000 and bun_045) are depicted in Figs. 3(c-d), when the convergence criterion is satisfied.

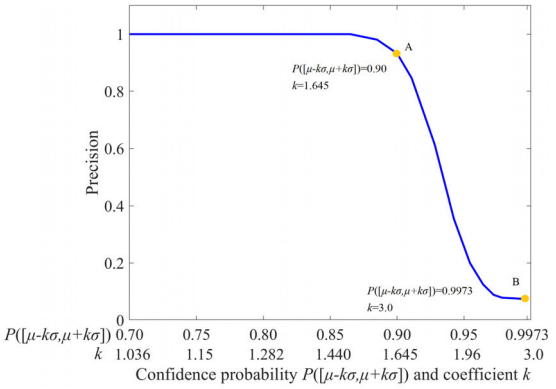

FIGURE 5. The relation between the confidence probability and precision. Precision = No. of correct matches/No. of matches and the correspondences are acceptable, if their distance is less than 3×mr (mr: mesh resolution) in accurate registration.

D. FLOWER POLLINARION ALGORITHM (FPA)

Inspired by the pollination phenomenon of phanerogam, Yang proposed a heuristic method-flower pollination algorithm (FPA) [33]. For optimal reproduction, the method of follower pollination can be mainly divided into cross-pollination and self-pollination. Cross-pollination is pollen intercourse between different flowers, which is the consequence of biotic and natural factors, while self-pollination is the opposite. Following these, the main rules can be listed as follows (13), as shown at the bottom of the page.

R. 1: The global search process is derived from cross-pollination and the movement of pollinators according with levy flight behavior.

R. 2: The local search process stems from self-pollination.

R. 3: The reproduction probability is proportional to the similarity of two flowers involved in pollination, which is equivalent to flower constancy provided by pollinators.

R. 4: The convention between the cross-pollination and self-pollination is controlled by a switch probability $prob_{\mathrm{FPA}} \in [0,1]$ with a small bias towards self-pollination.

Following R. 1 and R. 3, the global search process can be represented by

$$\begin{cases} p_k^{t+1} = p_k^t + L(\lambda)(p_k^t - p_{best}^t) \\ L \sim \dfrac{\lambda\Gamma(\lambda)\sin(\pi\lambda/2)}{\pi}\dfrac{1}{s^{1+\lambda}} \end{cases} \quad (s \gg s_0 > 0), \tag{14}$$

where p_k^t indicates the position of pollen k at the t-th iteration, and p_{best}^t is the position of the current best solution, and $L(\lambda)$ is the Levy flights-based step size, which is used to simulate the approximate Levy distribution, $\Gamma(\lambda)$ is the standard gamma function. As mentioned in Ref. [34], the method is also effective, when minimum step size s_0 is less than 0.1. Thus the critical size s_0 is 1E-3 in proposed method, and step

$$\overrightarrow{e_{\lambda_{\min}}} = \begin{cases} \overrightarrow{e_{\lambda_{\min}}} & \sum_{j}^{\|x_j - x_i\| \le radius} \left(radius - \|x_j - x_i\|\right)(x_j - x_i)'\overrightarrow{e_{\lambda_{\min}}} > 0 \\ -\overrightarrow{e_{\lambda_{\min}}} & otherwise \end{cases} \tag{11}$$

$$\begin{cases} T_{iter} = mean(\overrightarrow{xy}_{R,iter}) \\ \overrightarrow{xy}_{R,iter} = \left\{ \overrightarrow{x_i y_{x_i} R,iter} \;\middle|\; \left\| \overrightarrow{x_i y_{x_i} R.iter-1} - mean(\overrightarrow{xy}_{R,iter-1}) \right\| \le k\delta(\overrightarrow{xy}_{R,iter-1}) \right\} \\ mean(\overrightarrow{xy}_{R,iter-1}) = \dfrac{1}{N_{iter-1}} \sum_{i=1}^{N_{iter-1}} \overrightarrow{x_i y_{x_i} R,iter-1} \\ \delta(\overrightarrow{xy}_{R,iter-1}) = \sqrt{\sum_{i=1}^{N_{iter-1}} \left(\overrightarrow{x_i y_{x_i} R.iter-1} - mean(\overrightarrow{xy}_{R,iter-1}) \right)^2 \Big/ (N_{iter-1} - 1)} \end{cases} \tag{13}$$

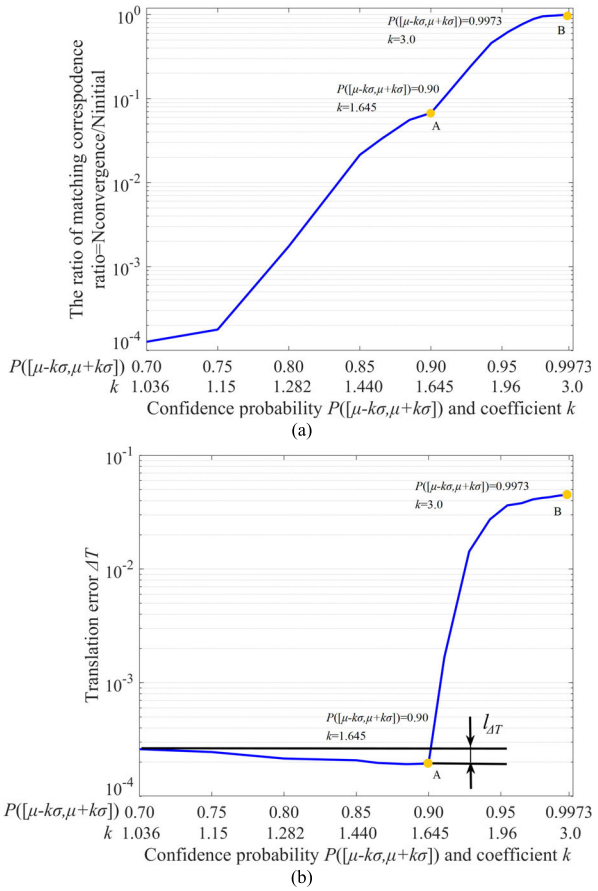

FIGURE 6. **The analysis of confidence probability. (a) the relation between confidence probability and matching counts. (b) the relation between confidence probability and translation error. In Fig. 6b, the translation error $\Delta T = ||T_{convergence} - T_{bench}||$.**

size s can be generated as following:

$$\begin{cases} s = u \Big/ |v|^{\frac{1}{\lambda}}, \quad u \sim N(0, \delta^2), v \sim N(0, 1) \\ \delta = \Gamma(1+\lambda) \cdot \sin(\dfrac{\pi\lambda}{2}) \Big/ \left[\Gamma\left(\dfrac{1+\lambda}{2}\right) \cdot \lambda \cdot 2^{\frac{\lambda-1}{2}} \right] \end{cases} \tag{15}$$

In Eq.15, u and v are the random numbers and subjected to the Gauss distribution. And λ is constant, which is generally set to 1.5. A new control parameter based on the prior work is introduced into the heuristic method to find a promising region in the early iterations and implement the fine-tuning of individuals in the final generations [35]. Thus, in our method, the local search strategy can be rewritten as

$$p_k^{t+1} = p_k^t + \varepsilon(t) \cdot (p_m^t - p_n^t), \tag{16}$$

where p_m^t and p_n^t are the pollens from different flowers at the t-th iteration. $\varepsilon(t)$ is subjected to a uniform distribution in $[0, g(t)]$, and g(t) can be calculated as

$$g(t) = \gamma_{\max} \exp\left(\log(r_{\min} \big/ r_{\max}) \cdot t \big/ t_{\max\_iter}\right) \tag{17}$$

In Eq. 17, $r_{\max}$ and $r_{\min}$ are the search radiuses in the early and final iterations, respectively ($r_{\max} = 0.3\pi$, $r_{\min} = 0.06\pi$), and $t_{\max\_iter}$ is the maximum iteration number.

E. POINT SET REGISTRATION VIA FPA AND PROPOSED METHOD

The pseudo-codes of the registration method based on standard FPA and the proposed method are shown in Figs. 7 and 8 respectively, for further discrimination.

Step.1. Input: point clouds Y(model) and X
The bound of population $r. \in$ [-180 °180°] and $t. \in [t_{\min}, t_{max}]$
Step.2. Initialization population:
Every pollen

$$p_i = \begin{cases} [0, 0, 0, 0, 0, 0] \text{current position} & i = 1 \\ [r_x, r_y, r_z, t_x, t_y, t_z] \ \text{random}(1, 6) & i = 2, \ldots, \text{pop\_num} \end{cases}$$

Normalization of pollen p_i in range [-1 1];
Fitness(p_i)=RMSE[p_i, X, Y] after denormalization
Best Fitness, Id_{best}
Step.3. While (Not reached stop criterion)
For i=1,2,…,pop_num
If random(0, 1)>$prob_{\text{FPA}}$
p_i^{t+1}=global research(p^{t+1}) (Eq.14)
Else: p_i^{t+1}=local research(p^{t+1}) (Eq.16)
End If
Fitness($p^{t+1}{}_i$)=RMSE($p^{t+1}{}_i$, X, Y) after denormalization;
Updata Fitness(p_i), p_i, Best Fitness, Id_{best}
End for
End while
Output: $R(r_x, r_y, r_z)$, $T(t_x, t_y, t_z)$

FIGURE 7. **pseudo-code of FPA used for point set registration.**

As the introduction in prior studies [5]–[7], the pseudo-code of FPA in six dimension optimization is shown in Fig. 7, and the procedure of the proposed method is listed in Fig. 8. Compared with the traditional method, the proposed method finds the optimal solution in the rotation space (Step 1 in Figure 8a), and the translations between the models can be derived from the Pauta sub-function. In heuristic methods, the search space is always truncated, which means the pollens stop at the boundary, when they overstep the boundary, as represented in Eq.18. Considering the periodicity of searching space in our method, the truncated boundary is replaced by cycle boundary (Step a in Fig. 8a), which can be denoted as Eq.19.

$$p_{i,j} = \begin{cases} Lb_j & p_{i,j} < Lb_j \\ Ub_j & p_{i,j} > Ub_j \end{cases} \tag{18}$$

$$p_{i,j} = \begin{cases} Ub_j - mod(Lb_j - p_{i,j}, 2\pi) & p_{i,j} < Lb_j \\ Lb_j - mod(p_{i,j} - Ub_j, 2\pi) & p_{i,j} > Ub_j \end{cases} \tag{19}$$

In the above equations, $p_{i,j}$ is the elements j in pollen i, and $mod()$ is the mod operation, and Ub_j and Lb_j are the upper and lower bounds for elements j. To demonstrate the effects of proposed strategy, the bunny model, depicted in Fig. 11a, is selected as registration objects. Each method is run 50 times randomly and independently. As demonstrated in Table 1, the proportion of optimal pollens in proposed strategy is higher than other strategies. And the strategy involved with fixed search radius and truncated boundary only has a higher proportion of optimal pollens, when the best solution is close to the boundary. As depicted in Fig. 9a, the pollens are disorder and many of them are located in boundary for standard FPA. Once the cycle boundary involved, the pollens have

TABLE 1. Proportion of optimal pollens after registration.

	TR1	TR2	TR3
fixed search radius $r(r=r_{max})$ + truncated boundary	34%	28%	48%
fixed search radius r ($r=r_{max}$)+ cycle boundary	47%	52%	38%
contractive search radius (Eq.16) + cycle boundary	57%	63%	52%

Step.1. **Input:** point clouds Y(model) and X, and their normal Eq. (9-10)
The bound of population [-180 °180°]
Step.2. Initialization population:
Every pollen

$$p_i=\begin{cases}\text{current position} & i=1\\ \text{random(1,3) in population bound} & i=2,\ldots,pop\_num\end{cases}$$

Fitness(p_i)= **Pauta** (p_i, Y, X, normal(Y), normal(X));
Best Fitness, Id_{best}
Step.3. While (Not reached stop criterion)
For i=1,2,…,pop_num
If random(0, 1)>$prob_{FPA}$ ($prob_{FPA}$=0.7)
p_i^{t+1}=global research(p^{t+1}) (Eq.14)
Else: p_i^{t+1}=local research(p^{t+1}) (Eq.16-17)
End If
Step *a* : p_i^{t+1}=cyclebound (p_i^{t+1},Lb,Ub)
Fitness(p^{t+1}_i)=**Pauta** (p^{t+1}_i, Y, X, normal(Y), normal(X));
Updata Fitness(p_i), p_i, Best Fitness, Id_{best}
End for
End while
Output: $R(r_x,r_y,r_z)$, $T(t_x,t_y,t_z)$

(a) main stream of the proposed registration method

Fitness(p_i)= **Pauta** (p_i, Y, X, normal(Y), normal(X))
Normal(X,R)=R·normal(X);
Find the nearest normal vector of normal(X,R) in normal(Y) with kd-tree technology
Step *a* : $\overrightarrow{xy}_R=\{\overrightarrow{x_i y_{x_i R}}\,|\,a\cos[normal(x_i,R),normal(y_{xi})]<15°\}$
Step *b* : If $num(\overrightarrow{xy}_R)<0.1\times\min[num(\mathrm{X}),num(\mathrm{Y})]$,
Fitness(p_i)=1.0E6, break;
For iter=1,…,iter_max (iter_max=60)
Updata $T_{iter},\overrightarrow{xy}_{R,iter},Mean(\overrightarrow{xy}_{R,iter}),\delta(\overrightarrow{xy}_{R,iter})$ according Eq. 13;
When $\delta(\overrightarrow{xy}_{R,iter})-\delta(\overrightarrow{xy}_{R,iter-1})<\delta(\overrightarrow{xy}_{R,iter-1})\times 0.1\%$, break;
End for
$Fitness(p_i)=\mathrm{RMSE}(\mathrm{Y},RX+T)$
for partial registration $\mathrm{RMSE}(\mathrm{X},\mathrm{Y})=\{(x_i,y_{xi})\,|\,\|Rx_i+T-y_{xi}\|<k\times\delta_{end}\}$

(b) Pauta sub-function used for fitness function evaluation

FIGURE 8. Pseudo-code of the proposed method for point registration.

more probabilities to find the optimal solution. Comparing to the methods, whose search radius is fixed, the failed pollens of proposed method are less.

To reduce the calculations and simplify the correspondences, two implementations are appended in the sub-function (Steps *a* and *b* in Figure 8b). In Step *a*, the correspondences, which have a quite deviation in the normal direction, are unreliable and should be removed from the volunteers. In Step *b*, the overlapping of the correspondences is considered, especially for the registration of the open surface. The solutions can be removed, if correspondence overlapping is too small, as shown in Fig. 10.

IV. EXPERIMENTS AND DISCUSSION

To investigate the performance of proposed method, the experiments in the initial position, noise, outliers, and partial overlapping are carried out. And, both deterministic methods and heuristic-based alignments are introduced for comparison.

A. TRADITIONAL REGISTRATION METHOD

To verify the robustness of the proposed method to position complexity in 3-D registration, synthetic models from Stanford 3D Scanning Repository, the UWA dataset [36], [37], and freeform parts in manufacturing are adopted as the registration models, which are demonstrated in Fig. 11. The handle and emergency-hammer come from 3D scanning. Moreover, as depicted in Fig.16a, the free-form surface comes from a traditional coordinate measurement machine (CMM). The number of extracted points is as follows: bunny has 8131 points, dragon has 8000 points, chef has 7992 points, handle has 8155 points, emergency-hammer has 5151 points, and free-form surface has 3321 points. For the unification of the models' sizes, each model is scaled into a cube box with a size of $[-1, 1]$. In the experiments, the target model is translated to the origin of the coordinate system, and the source model comes from the target model with Euclidean transformations. The Euclidean transformation is listed in Table 2. It should be noted that both rotation and translation are considered, which means that the center of the source model is not consistent with the target model's center before registration.

In the experiments, the deterministic methods that are used for comparison are ICP [10], ICPP, CPD [11], IRLS [38], and SDRSAC [16]. And the heuristic methods are ABC [39], bat-inspired algorithm (BA) [40], cuckoo search (CS) [41], DE [42], FPA [32], GA [43], HS [44], and particle swarm optimization (PSO) [45]. The parameters of ABC are as follows: CS = 30 and limit = 180. The parameters of BA are set follows: population size (PS) = 30, pulse emission ratio = 0.9, and the loudness coefficient is 0.8. The parameters of CS are as follows: PS = 30 and the discovery rate of alien eggs is 0.25. The parameters of DE are as follows: PS = 30, the mutation coefficient mc$\in$U [0,1], and the cross-rate CR = 0.8. The parameters of FPA and the proposed method are as follows: PS = 30 and $Prob_{\mathrm{FPA}} = 0.7$. The parameters of GA are as follows: PS = 100, crossover rate cr = 0.5 and the mutation ration $mr = 0.1$. The parameters of HS are set as follows: PS = 30, HMCR = 0.95, bw = 0.2, and PAR = 0.3. The parameters of PSO are as follows: PS = 40, the learning coefficient $c_1 = c_2 = 1.5$ and the weight factor $w = 0.85$.

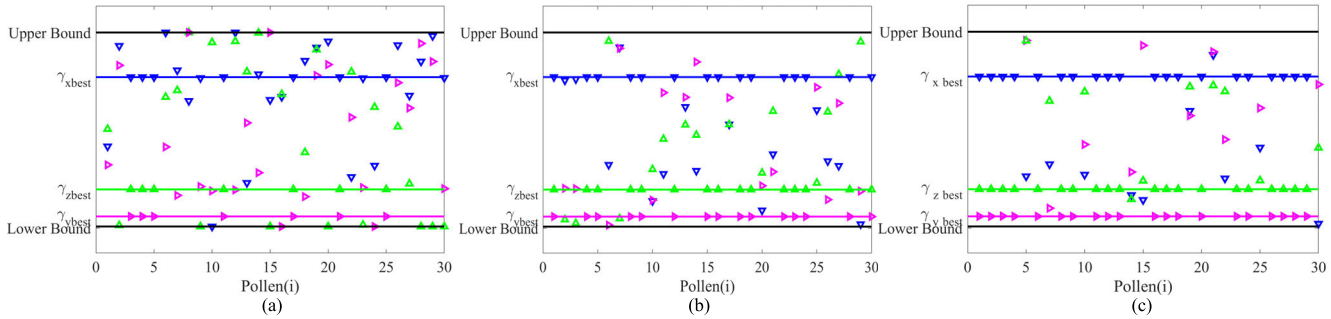

FIGURE 9. The pollens distribution after registration (TR2). (a) the proposed method with fixed search radius r and truncated boundary. (b) the proposed method with fixed search radius r and cycle boundary. (c) the proposed method with contractive search radius r (Eq.17) and cycle boundary.

TABLE 2. The initial position between the source and target models.

Trans. No	R_x (°)	R_y (°)	R_z (°)	T_x (mm)	T_y (mm)	T_z (mm)
TR1	30	30	30	L/20	L/20	L/20
TR2	60	60	0	L/2	L/2	L/2
TR3	170	170	0	L	L	L

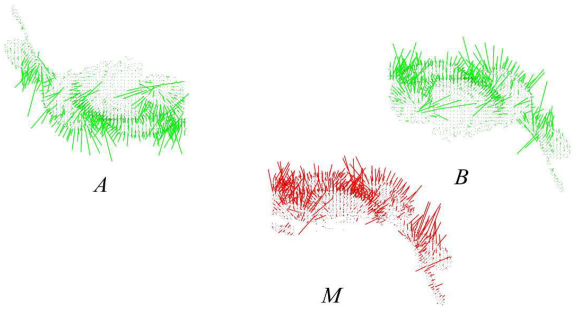

FIGURE 10. The analysis of the correspondences overlapping (bunn_000 in red, and bun_045 in green). Compared wtih position B, the normal directions in position A are mostly different from the ones in position M, and their overlapping is smaller than that in position B.

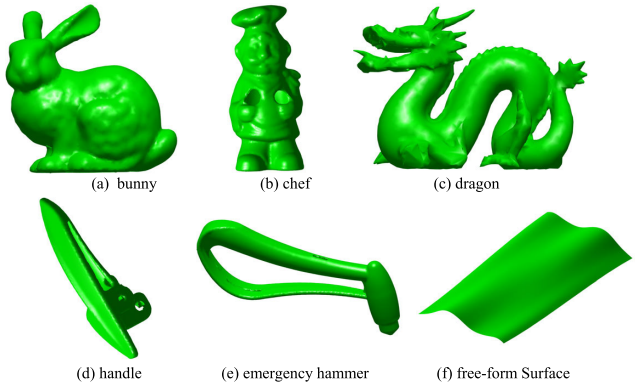

FIGURE 11. Synthetic models used for registration in single-float type.

For all the heuristic methods, the number of function evaluations (FEs) is 40000, and each population is normalized in the range $[-1, 1]$. The maximum iterations of ICP, ICPP, and CPD are 60, and the parameter settings of IRLS and SDRSAC are referenced in the prior work [16], [37].

All the methods are implemented with MATLAB R2017b and are run on the same Intel(R) Core(TM) i7-9800X CPU @ 3.80 GHz with 16 GB RAM and Windows 10 operating system. According to the above setting in Fig.1, the upper and lower bounds of the traditional heuristic method can be described as Eq. 20, as shown at the bottom of the next page.

The upper and lower bounds of the proposed method are $UB = [180°, 180°, 180°]$ and $LB = [-180°, -180°, -180°]$. To further improve the registration accuracy, the standard FPA is used for refinement after the proposed method, and its bounds are $[-5°, 5°]$ and $[-5mr, 5mr]$. The FEs number of the proposed method and refinement are 24000 and 16000, and they are represented by Proposed-I and Proposed-II in Fig.12.

To demonstrate the robustness to the initial position, the convergence results of the compared methods are presented in Fig.12 and Table 3, and the points in the process are the single-float type. The registration is acceptable if the value of RMSE is smaller than 1.0E-5, which is highlighted in bold in Table 3. For the heuristic methods, the current position is one of the initial solutions. As shown in Fig.12, some heuristic methods and local optimizations can also achieve registration when the initial status is simple. For example, the results of bunny in TR1 are as follows: 5.40E-8 (ABC), 5.40E-08 (BA), 8.50E-08 (CS), 1.00E-07 (DE), 8.50E-08 (FPA), 1.58E-02 (GA), 1.79E-03 (HS), 5.02E-04 (PSO), and 6.35E-08 (proposed method). The convergence results of the heuristic optimizations, such as ABC, BA, CS, DE, FPA, and the proposed method, are more close and much better than the others as well as local optimizations. When the initial position is complex, most of the traditional methods are trapped by local optimizations; while, the proposed method can find better solutions. For example, when the initial positions are TR2

TABLE 3. Registration results of each model based on heuristic optimizations and deterministic methods.

Method		ICP	ICPP	CPD	IRLS	SDRSAC	ABC	BA	CS	DE	FPA	GA	HS	PSO	Proposed
Bunny	TR1	**6.38E-07**	**9.10E-08**	**5.42E-08**	**4.06E-08**	**3.28E-07**	**5.40E-08**	**5.40E-08**	**8.50E-08**	**1.00E-07**	**8.50E-08**	1.58E-02	1.79E-03	5.02E-04	**6.35E-08**
	TR2	1.54E-01	1.51E-01	1.86E-01	1.51E-01	**1.16 E-06**	1.87E-01	**1.02E-07**	1.28E-01	1.85E-01	1.80E-01	1.87E-01	1.74E-01	5.02E-04	**1.01E-07**
	TR3	1.70E-01	1.74E-01	1.74E-01	1.70E-01	**1.09 E-06**	1.02E+00	2.21E-01	1.52E-01	1.71E-01	1.22E-01	2.26E-01	1.73E-01	1.51E-01	**1.75E-07**
Chef	TR1	1.28E-02	**7.06E-08**	**4.81E-08**	2.15E-02	**4.19 E-07**	1.03E-03	**4.86E-08**	1.51E-02	4.16E-02	**8.75E-06**	4.32E-02	4.39E-02	4.54E-02	**7.02E-08**
	TR2	4.50E-02	**1.40E-07**	4.45E-02	4.51E-02	1.30E-02	1.14E-01	8.12E-02	4.24E-02	7.83E-02	4.80E-02	9.00E-02	4.71E-02	8.01E-02	**9.62E-08**
	TR3	7.69E-02	7.67E-02	8.38E-02	7.72E-02	1.54E-02	1.15E+00	5.28E-02	4.87E-02	9.14E-02	8.66E-02	2.19E-01	9.10E-02	4.57E-02	**1.68E-07**
Dragon	TR1	**5.97E-07**	**7.05E-08**	**4.52E-08**	1.06E-01	**4.89 E-07**	**4.52E-08**	**4.52E-08**	**1.51E-07**	1.06E-01	**7.46E-08**	5.37E-03	2.33E-03	9.31E-02	**5.71E-08**
	TR2	9.42E-02	1.12E-01	**9.61E-08**	1.53E-01	**3.93 E-06**	1.78E-01	1.12E-01	9.33E-02	1.12E-01	1.01E-01	1.09E-01	9.55E-02	1.72E-01	**9.45E-08**
	TR3	9.95E-02	9.63E-02	1.11E-01	1.17E-01	**1.07 E-06**	1.09E+00	2.80E-01	1.14E-01	5.44E-02	5.29E-02	1.35E-01	1.73E-01	2.04E-02	**1.72E-07**
Handle	TR1	1.20E-02	**8.28E-08**	**3.28E-08**	1.72E-02	**2.02E-06**	**3.31E-08**	**3.31E-08**	**5.53E-08**	**3.08E-08**	3.48E-02	1.31E-02	1.66E-03	1.49E-03	**4.27E-08**
	TR2	1.21E-02	1.18E-01	**8.73E-08**	1.77E-02	1.24E-01	2.02E-01	**1.99E-07**	9.45E-02	1.25E-01	1.40E-01	1.33E-01	1.46E-01	1.28E-01	**8.74E-08**
	TR3	8.86E-02	8.83E-02	1.16E-01	9.83E-02	**1.48 E-06**	9.07E-01	3.89E-02	1.38E-01	1.36E-01	1.36E-01	2.62E-01	1.46E-01	1.55E-01	**1.74E-07**
Emergency hammer	TR1	1.07E-02	**1.02E-07**	**4.99E-08**	1.10E-02	1.10E-02	1.00E-04	**5.44E-08**	2.64E-03	7.60E-02	1.92E-02	2.08E-02	7.59E-02	7.60E-02	**5.55E-08**
	TR2	1.07E-02	**1.05E-07**	**9.06E-08**	1.08E-02	1.10E-02	1.31E-01	1.36E-01	5.23E-02	7.64E-02	7.63E-02	8.32E-02	1.13E-01	7.78E-02	**1.06E-07**
	TR3	8.50E-02	7.60E-02	1.43E-01	8.51E-02	1.10E-02	9.17E-01	2.19E-01	4.61E-02	1.74E-01	1.64E-01	3.69E-01	1.45E-01	1.35E-01	**1.68E-07**
Surface	TR1	4.86E-01	**1.51E-07**	7.25E-01	4.81E-01	2.88E-02	4.81E-03	3.03E-03	2.39E-05	5.51E-02	**2.12E-06**	5.68E-02	5.97E-02	2.49E-03	**6.52E-08**
	TR2	7.13E-01	2.47E+01	2.46E+00	7.14E-01	1.80E-02	1.64E-01	3.03E-03	5.83E-02	9.19E-02	1.98E-02	1.23E-01	1.04E-01	5.69E-02	**9.40E-08**
	TR3	9.85E-01	2.99E+01	3.64E+00	1.47E+00	2.74E-02	9.90E-01	1.25E-02	5.93E-02	4.30E-02	1.20E-01	2.62E-01	2.62E-02	1.14E-02	**1.70E-07**

and TR3, the heuristic optimizations that found solutions in the six-dimensional space cannot align the models perfectly in most cases.

As listed in Table 3, CPD and SDRSAC have a higher chance of achieving precise registration than the other local optimizations. Unlike the settings mentioned in the prior work [5]–[7], both rotation and translation are our main considerations. In our experiments, the pervious heuristic methods are more likely to fail to alignment, and their performance is even inferior to local optimizations when the initial position is complex. However, compared with the other methods, the registration results of the proposed method are satisfied in all the cases.

B. EXPERIMENTS WITH NOISE

To verify the registration robustness to noise, Fig. 13 evaluates the registration results of different methods concerning noise. The registration object is bunny, and the initial position is depicted in Fig. 13*a*. In the experiment, the target model is in green, and the source model is in red and deteriorated by Gaussian noise. The rotation and translation errors, written in Eq. 21, are used for evaluation, and all the methods are implemented ten times independently and randomly, where *trace*() refers to the trace operator of matrix. In Figs. 13(*b*-*c*), the number in the x-axis denotes the ratio between the standard deviation and mesh resolution.

$$\begin{cases} \theta_{error} = a\cos\left(0.5 \times \left(trace(R \cdot R'_{bench}) - 1\right)\right) \times 180^{\circ}/\pi \\ T_{error} = \|T - T_{bench}\| \end{cases} \tag{21}$$

As demonstrated in Fig. 13, the noise affects the registration accuracy, and the errors increased gradually with the rise of the standard deviation. Compared with ICP, ICPP, IRLS, and SDRSAC, the proposed method and CPD are more robust and consistent against noise, and the performance of CPD is better. The estimated errors with a standard deviation of $\delta_{\text{source}} = 0.5$mr for ICP, ICPP, IRLS, CPD, SDRAC and the proposed method are 0.223, 0.0523, 0.328, 0.0409, 0.0994, and 0.0493 (degree) in rotation and 5.91e-4, 2.17e-4, 9.15e-4, 1.66e-4, and 5.81e-4, 2.09e-4 (L) in translation.

C. EXPERIMENTS WITH OUTLIERS

To identify the performance against outliers, the registration results of the different methods are depicted in Fig. 14.

$$\begin{cases} UB = [\,180^{\circ}\ 180^{\circ}\ 180^{\circ}\ dist(center(\mathrm{X})) + L/2\ dist(center(\mathrm{X})) + L/2\ dist(center(\mathrm{X})) + L/2\,] \\ LB = [\,-180^{\circ}\ -180^{\circ}\ -180^{\circ}\ -dist(center(\mathrm{X})) - L/2\ -dist(center(\mathrm{X})) - L/2\ -dist(center(\mathrm{X})) - L/2\,] \end{cases} \tag{20}$$

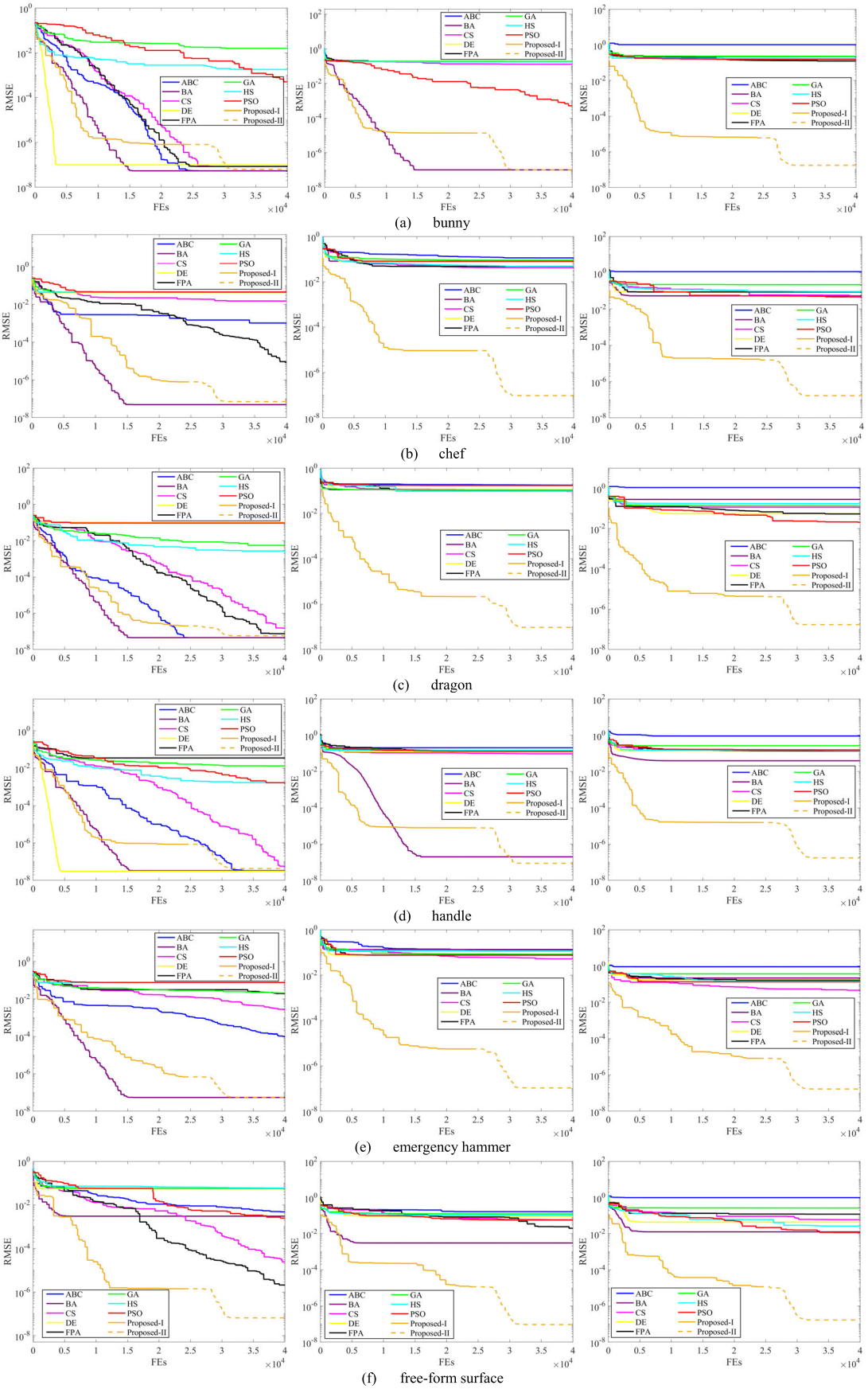

FIGURE 12. Convergence comparison of the heuristic methods (from left to right: TR1, TR2, and TR3).

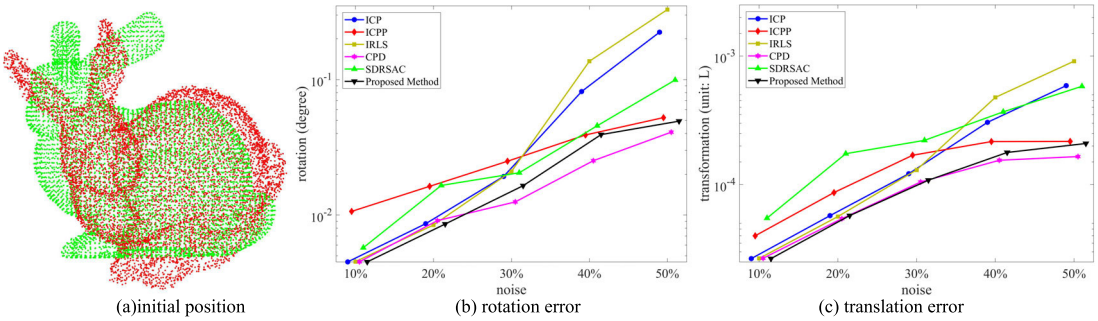

(a)initial position (b) rotation error (c) translation error

FIGURE 13. Comparisons of different methods against noise interference.

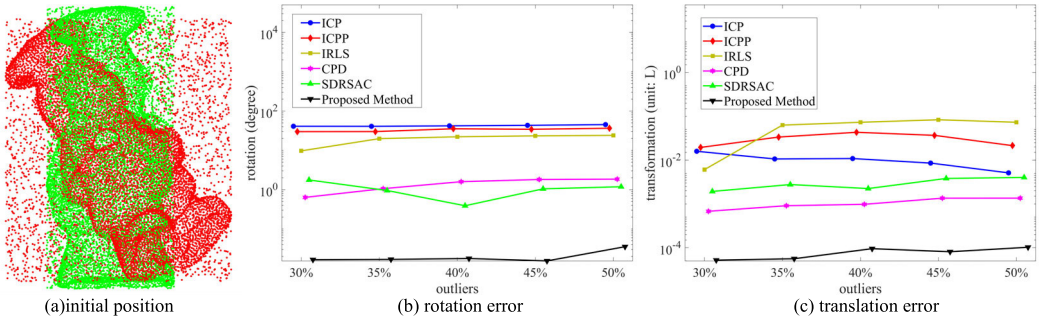

(a)initial position (b) rotation error (c) translation error

FIGURE 14. Comparisons of different methods against outliers.

The registration object is the chef model, and the initial position is shown in Fig. 14a. The outliers are uniform discrete points, which located in the external-tangent box of the model. The evaluations come from the rotation and translation error, and all methods are also run ten times randomly. In Figs. 14(b-c), the number in the x-axis denotes the ratio between the numbers of the outliers and the point set.

As shown in Figs. 14(b-c), compared with ICP, ICPP, and IRLS, the robust registration methods, such as CPD and SDRAC, are more robust to outliers. However, the performance of the proposed method is much better than other methods. For example, the estimated error of ICP, ICPP, IRLS, CPD, SDRSAC, and proposed method are: 45.2, 36.5, 24.1.1.85, 1.19, and 0.0354 (degree) in rotation and 5.11e-3, 2.15e-2, 7.31e-2, 1.36e-3, 4.03e-3, and 1.03e-4 (L) in translation, when the ratio of outlier is 50%. The estimated error of the proposed method is much less than other methods.

D. EXPERIMENTS IN 3D MODELING

To identify the registration performance in 3D modeling, Tables 4-5 demonstrate the quantitative comparison with different models from the Bologna dataset [46]. With the help of the reference rigid transformation provided in Bologna, it is feasible to estimate registration results by the rotation and translation error, and their initial positions are depicted in Fig. 15*a*. For better observation, the scenes, such as bunny, dragon, and armadillo, are displayed in different colors. Considering that the median square error (MedSE) is usually used as an objective function in 3D modeling [8], [9], it is also introduced in FPA and denoted as FPA-median in this part. For FPA-median, both the source and target models are translated to the origin of the coordinate system using their centers to reduce the computation in translation searching. The scenes, in which the overlapping ratio is larger than 40%, are applied as registration objects. The overlapping ratio can be calculated by Eq. 22, as shown at the bottom of the page.

To improve the calculation speed, the point set, used in registration, comes from the uniform down-sampling of the scene. The mean values of θ_{error} and T_{error} are listed in Tables 4-5. For the proposed method, there are no refinements involved in the process. In most cases, the results of the proposed method are closer to the benchmark than other methods. For example, in 3D modeling of Dragon, the estimated error of ICP, ICPP, CPD, FPA-median, SDRSAC, and the proposed method are: 11.91, 17.54, 8.653, 19.09, 6.052, and 0.3014 (degree) in rotation and 0.2442, 0.2978, 0.2100, 0.2446, 0.0424, and 0.0049 (L) in translation. In the mario model, SDRAC have better performance than our method.

$$\text{Overlapping Ratio} = \frac{\text{No. of corresponding points in X and Y}}{\text{sum (No. of points in X and Y)} - \text{No. of corresponding points in X and Y}} \tag{22}$$

TABLE 4. Rotation error.

Rotation (°)	bunny	dragon	armadillo	mario	squirrel	frog
ICP	66.94	11.91	30.01	101.4	94.51	88.18
ICPP	66.11	17.54	39.56	98.56	97.32	91.55
CPD	45.20	8.653	29.12	78.66	96.81	101.28
FPA-median	26.41	19.09	4.048	23.85	45.74	13.62
SDRSAC	14.46	6.052	1.676	**1.417**	37.25	1.0813
Proposed Method	**0.4479**	**0.3014**	**0.3053**	1.881	**1.309**	**0.8776**

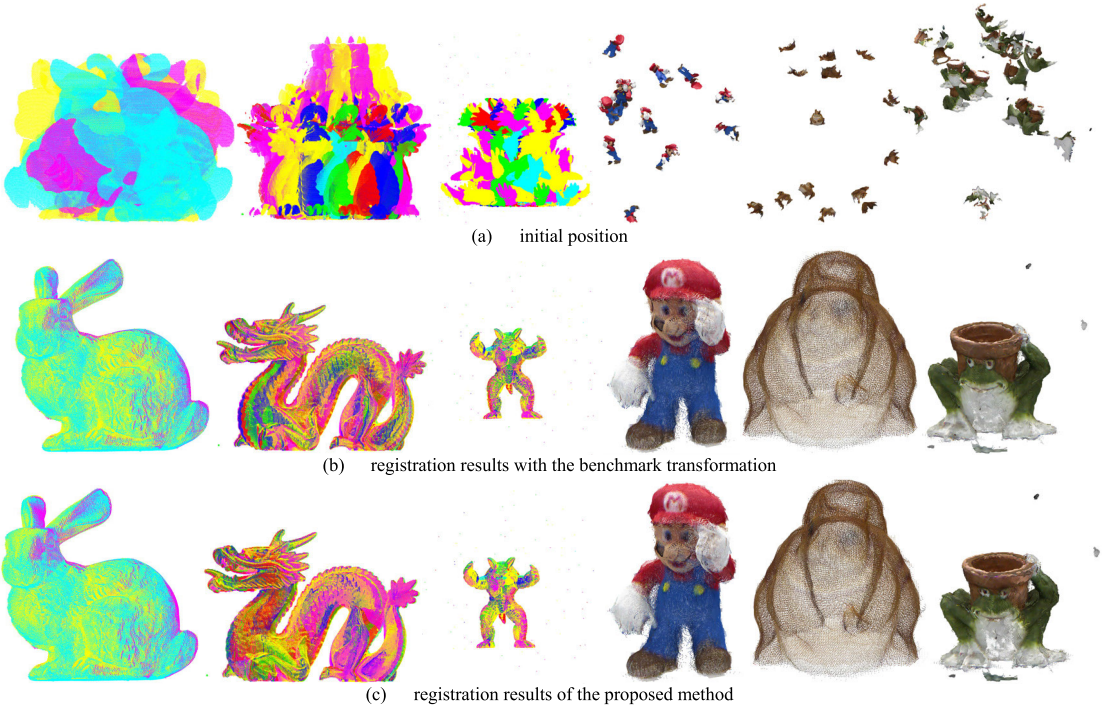

(a) initial position

(b) registration results with the benchmark transformation

(c) registration results of the proposed method

FIGURE 15. The registration results of the partial-overlapping scenes.

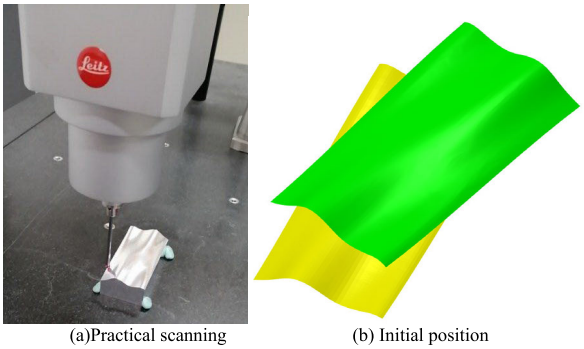

(a)Practical scanning (b) Initial position

FIGURE 16. Registration model and initial position.

However, its result is poor and unacceptable in the modeling of bunny and squirrel.

In Fig. 15, the reconstruction results of the benchmark transformation and proposed method are depicted. Our reconstruction is close to the benchmark, even when the initial position is complex.

E. APPLICATION IN QUALITY INSPECTION

The parts with free-form surface have been widely used in aerospace, automotive and shipbuilding industry. The free-form part is an essential element in manufacturing. However, it is hard to evaluate machine errors of free-form parts due to the lack of exact references. Registration, as a critical process in the inspection system, has been studied for decades.

An open free-form surface, depicted in Fig. 16a, is used as the registration object (100mm×50mm×10mm). To improve the scanning precision, the part is placed on the anti-vibration platform and scanned with a coordinate measuring machine (CMM, Leitz Metrology, Reference 600). The scanning model has 3200 points (sample interval: 1.25mm×1.25mm). The CAD model has 157641 points (sample interval: 0.178mm×0.178mm). Their initial positions are demonstrated in Fig. 16b. The CAD model is in green and regarded as the target model in registration, and the yellow one represents the scanning model.

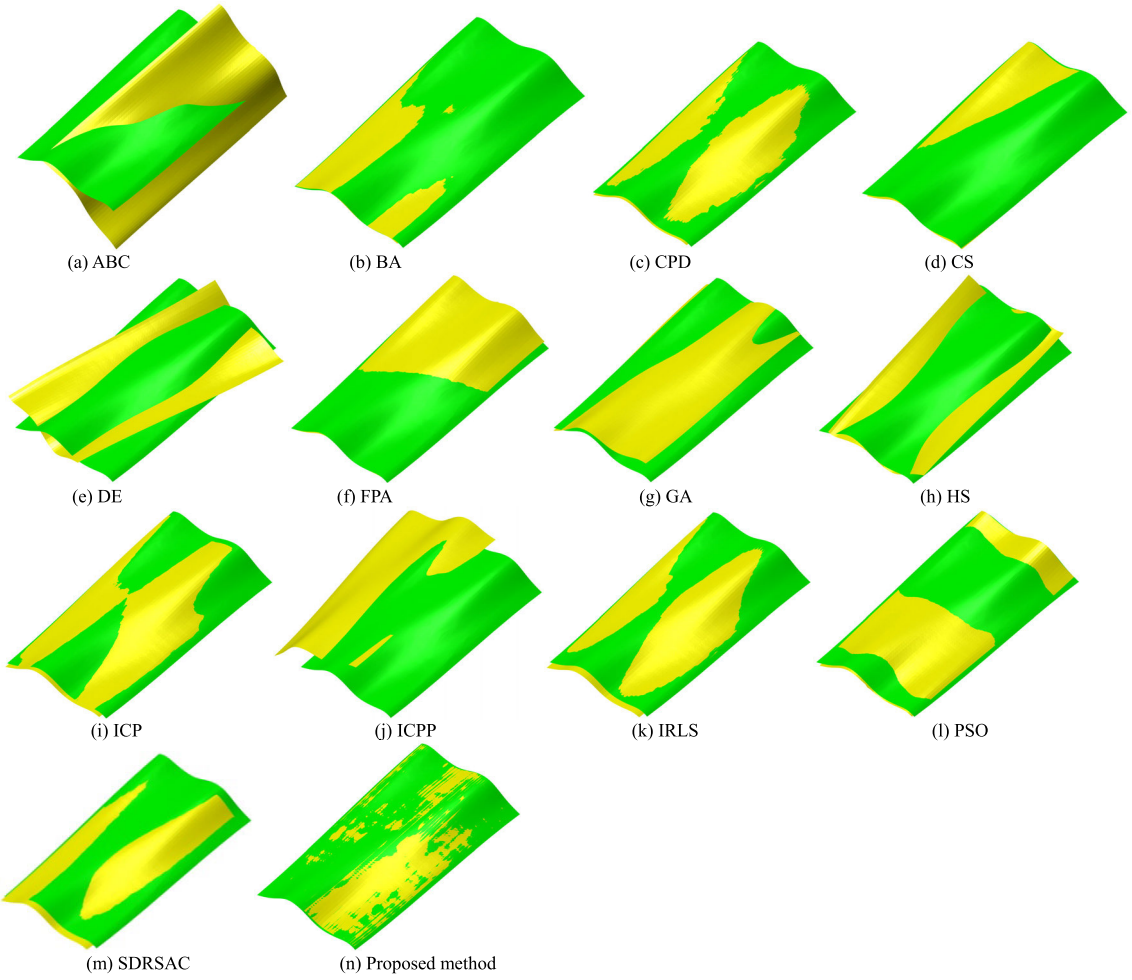

FIGURE 17. Registration result of free-form surface.

TABLE 5. Translation error.

Transformation (unit: L)	**bunny**	**dragon**	**armadillo**	**mario**	**squirrel**	**frog**
ICP	0.7930	0.2442	0.3601	4.0395	4.9638	2.5689
ICPP	0.8051	0.2978	0.3222	3.3093	5.3208	2.9749
CPD	0.2835	0.2100	0.2937	2.5566	4.0608	3.7945
FPA-median	0.2562	0.2446	0.0979	0.5089	2.1954	0.6754
SDRSAC	0.0990	0.0424	0.0098	**0.0937**	1.3700	0.0445
Proposed Method	**0.0043**	**0.0049**	**0.0044**	0.1128	**0.0651**	**0.0373**

TABLE 6. Comparison of the registration results.

Method	ABC	BA	CS	DE	FPA	GA	HS
RMS(mm)	9.3761	0.0758	0.2258	3.9132	0.8802	2.4568	0.8371
Method	PSO	ICP	ICPP	CPD	IRLS	SDRSAC	Proposed
RMS(mm)	0.6184	0.3133	12.221	0.2188	0.2180	0.5286	0.0547

The comparison results are depicted in Fig. 17. The deterministic methods, such as ICP, ICPP, CPD, IRLS, and SDRSAC, are trapped in local optimum and failed to align. Especially for ICPP, there are serious distortions in its registration. In the heuristic methods, the results of DE and HS are also distorted. In their alignments, the directions of the aligned surfaces are opposite. Other heuristic methods are more or less incapable of meeting the registration accuracy.

Compared with the other methods, the registered surfaces contain more intersections and are splotchy.

We used the RMSE to evaluate the performance of the registration. Its reference value comes from the refinement in MeshLab, which is after manual interventions. To guarantee the reliability of the reference value, the above process is run ten times independently, and the minimum value is regarded as the reference value. According to the above steps, the ground truth is 0.0547 ($RMS_{bench} = 0.0547$mm).

The quantitative comparison of different methods is listed in Table 6. The alignment can be regarded as a successful result when the evaluated error is close to 0.0547 mm. In comparison with the other methods, the proposed method shows better accuracy and could meet the inspection requirements.

V. CONCLUSION

Previously, efforts are made with heuristic methods to find the optimal solution in bounded six-dimension space to fulfill the 3D registration. Moreover, a reasonable setting of the bounded spaces is important and indispensable to ensure the accuracy of alignment. However, it is still an empirical work, and it has rarely been discussed in related studies. Compared with rotation space, which is periodic, the setting of the translation space is more difficult, and it is always different in related studies.

According to the problems mentioned above, a normal-based FPA optimization is introduced to point set registration. In our method, the registration can be achieved by finding the optimal solution in rotation space. Due to the invariability of the normal distribution to translation, the closeness of the point normal is employed to find the correspondences between the points. Secondly, considering the deterioration of normal caused by the noise, outliers, scatter and occlusion in practical applications, the Pauta criterion based on a three-dimension vector is used to remove the abnormal point matching and refine the translation between the models. With the help of FPA, the optimal solution can be found in 3D space. Moreover, in order to increase the population of optimal pollens after convergence, the adjustment of searching radius and periodic boundary are introduced. To verify the performance of the proposed method, several experiments are conducted regarding to the initial position, robustness to noise and outliers, 3D modeling, and quality inspection of the free-form surface. From the quantitative analysis, our method shows better or competitive performance in robustness to abnormal disturbances and registration accuracy.

Although the proposed method can achieve the registration without any feature extraction or manual intervention, it should be admitted that the registration process based on the proposed method requires a certain amount of calculation. In practice, the efficiency can be improved by model simplification. The above-mentioned strategy, acquiring the point corresponds from the closeness of the point normal, can also be introduced into other heuristic methods, such as PSO, ABC and BA. And we will finish these studies in the future and investigate their applications in the alignment of structured scenes.

ACKNOWLEDGMENT

The authors would like to acknowledge Stanford University for providing the 3D models and Bologna University for providing the 3D scenes.

REFERENCES

[1] W. Li and P. Song, "A modified ICP algorithm based on dynamic adjustment factor for registration of point cloud and CAD model," *Pattern Recognit. Lett.*, vol. 65, pp. 88–94, Nov. 2015.
[2] S. de Sousa and W. G. Kropatsch, "Graph-based point drift: Graph centrality on the registration of point-sets," *Pattern Recognit.*, vol. 48, no. 2, pp. 368–379, Feb. 2015.
[3] Y. Li and P. Gu, "Free-form surface inspection techniques state of the art review," *Comput.-Aided Des.*, vol. 36, no. 13, pp. 1395–1417, Mar. 2004.
[4] M. Gong, S. Zhao, L. Jiao, D. Tian, and S. Wang, "A novel coarse-to-fine scheme for automatic image registration based on SIFT and mutual information," *IEEE Trans. Geosci. Remote Sens.*, vol. 52, no. 7, pp. 4328–4338, Jul. 2014.
[5] T. Li, L. Gao, P. Li, and Q. Pan, "An ensemble fruit fly optimization algorithm for solving range image registration to improve quality inspection of free-form surface parts," *Inf. Sci.*, vols. 367–368, pp. 953–974, Nov. 2016.
[6] T. Li, Q. Pan, L. Gao, and P. Li, "Differential evolution algorithm-based range image registration for free-form surface parts quality inspection," *Swarm Evol. Comput.*, vol. 36, pp. 106–123, Oct. 2017.
[7] T. Li, L. Gao, Q. Pan, and P. Li, "Free-form surface parts quality inspection optimization with a novel sampling method," *Appl. Soft Comput.*, vol. 62, pp. 550–570, Jan. 2018.
[8] J. Santamaria, S. Damas, O. Cordon, and A. Escamez, "Self-adaptive evolution toward new parameter free image registration methods," *IEEE Trans. Evol. Comput.*, vol. 17, no. 4, pp. 545–557, Aug. 2013.
[9] J. M. García-Torres, S. Damas, O. Cordón, and J. Santamaría, "A case study of innovative population-based algorithms in 3D modeling: Artificial bee colony, biogeography-based optimization, harmony search," *Expert Syst. Appl.*, vol. 41, no. 4, pp. 1750–1762, Mar. 2014.
[10] P. J. Besl and N. D. McKay, "A method for registration of 3-D shapes," *IEEE Trans. Pattern Anal. Mach. Intell.*, vol. 14, no. 2, pp. 239–256, Feb. 1992.
[11] A. Myronenko and X. Song, "Point set registration: Coherent point drift," *IEEE Trans. Pattern Anal. Mach. Intell.*, vol. 32, no. 12, pp. 2262–2275, Dec. 2010.
[12] C. K. Chow, H. T. Tsui, and T. Lee, "Surface registration using a dynamic genetic algorithm," *Pattern Recognit.*, vol. 37, no. 1, pp. 105–117, Jan. 2004.
[13] S. Rusinkiewicz and M. Levoy, "Efficient variants of the ICP algorithm," in *Proc. 3rd Int. Conf. 3-D Digit. Imag. Modeling*, Quebec City, QC, Canada, May/Jun. 2001, pp. 145–152.
[14] C. Zhang, S. Du, J. Liu, Y. Li, J. Xue, and Y. Liu, "Robust iterative closest point algorithm with bounded rotation angle for 2D registration," *Neurocomputing*, vol. 195, pp. 172–180, Jun. 2016.
[15] J. Yang, H. Li, D. Campbell, and Y. Jia, "Go-ICP: A globally optimal solution to 3D ICP point-set registration," *IEEE Trans. Pattern Anal. Mach. Intell.*, vol. 38, no. 11, pp. 2241–2254, Nov. 2016.
[16] H. M. Le, T.-T. Do, T. Hoang, and N.-M. Cheung, "SDRSAC: Semidefinite-based randomized approach for robust point cloud registration without correspondences," in *Proc. IEEE/CVF Conf. Comput. Vis. Pattern Recognit. (CVPR)*, Long Beach, CA, USA, Jun. 2019, pp. 124–133.
[17] Y. Yang, W. Chen, M. Wang, D. Zhong, and S. Du, "Color point cloud registration based on supervoxel correspondence," *IEEE Access*, vol. 8, pp. 7362–7372, 2020.
[18] L.-J. Fang, Z.-L. Sun, and K.-M. Lam, "An effective membership probability representation for point set registration," *IEEE Access*, vol. 8, pp. 9347–9357, 2020.
[19] B. Jian and B. C. Vemuri, "Robust point set registration using Gaussian mixture models," *IEEE Trans. Pattern Anal. Mach. Intell.*, vol. 33, no. 8, pp. 1633–1645, Aug. 2011.
[20] J.-J. Jacq and C. Roux, "Registration of 3-D images by genetic optimization," *Pattern Recognit. Lett.*, vol. 16, no. 8, pp. 823–841, Aug. 1995.

[21] K. Brunnstrom and A. J. Stoddart, "Genetic algorithms for free-form surface matching," in *Proc. 13th Int. Conf. Pattern Recognit.*, Vienna, Austria, vol. 4, 1996, pp. 689–693.
[22] C. Robertson and R. B. Fisher, "Parallel evolutionary registration of range data," *Comput. Vis. Image Understand.*, vol. 87, nos. 1–3, pp. 39–50, Jul. 2002.
[23] G. Dalley and P. Flynn, "Range image registration: A software platform and empirical evaluation," in *Proc. 3rd Int. Conf. 3-D Digit. Imag. Modeling*, Quebec City, QC, Canada, May/Jun. 2001, pp. 246–253.
[24] L. Silva, O. R. P. Bellon, and K. L. Boyer, "Precision range image registration using a robust surface interpenetration measure and enhanced genetic algorithms," *IEEE Trans. Pattern Anal. Mach. Intell.*, vol. 27, no. 5, pp. 762–776, May 2005.
[25] A. Valsecchi, S. Damas, J. Santamaría, and L. Marrakchi-Kacem, "Intensity-based image registration using scatter search," *Artif. Intell. Med.*, vol. 60, no. 3, pp. 151–163, Mar. 2014.
[26] I. De Falco, A. D. Cioppa, D. Maisto, and E. Tarantino, "Differential evolution as a viable tool for satellite image registration," *Appl. Soft Comput.*, vol. 8, no. 4, pp. 1453–1462, Sep. 2008.
[27] G. He, M. Zhang, and Z. Song, "Error evaluation of free-form surface based on distance function of measured point to surface," *Comput.-Aided Des.*, vol. 65, pp. 11–17, Aug. 2015.
[28] T. M. Tucker and T. R. Kurfess, "Newton methods for parametric surface registration. Part I. Theory," *Comput.-Aided Des.*, vol. 35, no. 1, pp. 107–114, Nov. 2001.
[29] T. M. Tucker and T. R. Kurfess, "Newton methods for parametric surface registration. Part II. Experimental validation," *Comput.-Aided Des.*, vol. 35, no. 1, pp. 115–120, Jan. 2003.
[30] W. L. Li, Z. P. Yin, Y. A. Huang, and Y. L. Xiong, "Three-dimensional point-based shape registration algorithm based on adaptive distance function," *IET Comput. Vis.*, vol. 5, no. 1, pp. 68–76, Jan. 2011.
[31] S. Salti, F. Tombari, and L. Di Stefano, "SHOT: Unique signatures of histograms for surface and texture description," *Comput. Vis. Image Understand.*, vol. 125, pp. 251–264, Aug. 2014.
[32] R. Bro, E. Acar, and T. G. Kolda, "Resolving the sign ambiguity in the singular value decomposition," *J. Chemometrics*, vol. 22, no. 2, pp. 135–140, Feb. 2008.
[33] X. S. Yang, "Flower pollination algorithm for global optimization," in *Proc. 11th Int. Conf. Unconventional Comput. Natural Comput.*, Sep. 2012, pp. 240–249.
[34] X. He, X.-S. Yang, M. Karamanoglu, and Y. Zhao, "Global convergence analysis of the flower pollination algorithm: A discrete-time Markov chain approach," in *Proc. Int. Conf. Comput. Sci.*, Jun. 2017, pp. 12–14.
[35] L. Wang, Y. Shi, and S. Liu, "An improved fruit fly optimization algorithm and its application to joint replenishment problems," *Expert Syst. Appl.*, vol. 42, no. 9, pp. 4310–4323, Jun. 2015.
[36] *Stanford 3D Scanning Repository*. Accessed: 2019. [Online]. Available: http://www-graphics.stanford.edu/data/3Dscanrep/
[37] A. S. Mian, M. Bennamoun, and R. Owens, "Three-dimensional model-based object recognition and segmentation in cluttered scenes," *IEEE Trans. Pattern Anal. Mach. Intell.*, vol. 28, no. 10, pp. 1584–1601, Oct. 2006.
[38] P. Bergström and O. Edlund, "Robust registration of point sets using iteratively reweighted least squares," *Comput. Optim. Appl.*, vol. 58, no. 3, pp. 543–561, Feb. 2014.
[39] D. Karaboga and B. Basturk, "A powerful and efficient algorithm for numerical function optimization: Artificial bee colony (ABC) algorithm," *J. Global Optim.*, vol. 39, no. 3, pp. 459–471, Oct. 2007.
[40] X. S. Yang, "A new bat-inspired algorithm," in *Nature Inspired Cooperative Strategies for Optimization (NICSO 2010)*, vol. 284. 2010, pp. 65–74.
[41] X. S. Yang and S. Deb, "Engineering optimization by cuckoo search," *Int. J. Math. Model. Numer. Optim.*, vol. 1, no. 4, pp. 330–343, Dec. 2010.
[42] R. Storn and K. Price, "Differential evolution—A simple and efficient heuristic for global optimization over continuous spaces," *J. Global Optim.*, vol. 11, no. 4, pp. 341–359, 1997.
[43] D. E. Goldberg, *Genetic Algorithms in Search Optimization and Machine Learning*. Reading, MA, USA: Addison Wesley, 2000.
[44] K. S. Lee and Z. W. Geem, "A new meta-heuristic algorithm for continuous engineering optimization: Harmony search theory and practice," *Comput. Methods Appl. Mech. Eng.*, vol. 194, nos. 36–38, pp. 3902–3933, Sep. 2005.
[45] J. Kennedy and R. C. Eberhart, "Particle swarm optimization," in *Proc. IEEE Int. Conf. Neural Netw.*, vol. 4, Nov./Dec. 1995, pp. 1942–1948.
[46] S. Salti, F. Tombari, and L. D. Stefano, "A performance evaluation of 3D keypoint detectors," in *Proc. Int. Conf. 3D Imag., Modeling, Process., Vis. Transmiss.*, Hangzhou, China, May 2011, pp. 236–243.

DING SHEN received the B.S. degree from the Jiangxi University of Science and Technology, China, in 2010, and the M.S. degree from Fuzhou University, China, in 2014, where he is currently pursuing the Ph.D. degree with the School of Mechanical Engineering and Automation. His research interests include free-form parts registration and inspection, surface characterization, and feature extraction of various materials.

YOUXI LIN received the Ph.D. degree from Fuzhou University, China, in 2007. He is currently a Professor with the School of Mechanical Engineering and Automation, and the Director of the Mechanical and Electrical Engineering Practice Center, Fuzhou University. He is also the Director of the Tribological Branch of the Chinese Mechanical Engineering Society; the Deputy Director of the Tribological Wear and Antifriction Materials and Technology Committee; a member of the Engineering Training Teaching Steering Committee of the Ministry of Education; and the Executive Vice President of the Fujian Tool Association, China. His research interests include the advanced manufacturing technology and the related tribology research.

ZHIYING REN received the B.S., M.S., and Ph.D. degrees from Fuzhou University, China, in 2003, 2006, 2015, respectively. She is the Deputy Director of the Youth Work Committee of the Tribological Branch of the Chinese Mechanical Engineering Society; and the Executive Director of the Fujian Automobile Association, China. She is currently an Associate Professor with the School of Mechanical Engineering and Automation, Fuzhou University. Her research interests include wear resistance, surface characterization and feature extraction of various materials; and research on fault diagnosis technology for various military vehicles.

WEIPING CHEN received the B.S. degree from Chang'an University, China, in 2012, and the M.S. degree from Fuzhou University, China, in 2015. He is a Full Member of the Chinese Mechanical Engineering Society, and currently a Faculty Member of the Mechanical and Electrical Engineering Practice Center, Fuzhou University. His research interests include the advanced manufacturing technology and the related engineering practical research.